Journal of Inorganic Biochemistry 195 (2019) 182–193

Contents lists available at ScienceDirect

Journal of Inorganic Biochemistry

journal homepage: www.elsevier.com/locate/jinorgbio

Vanadocene complexes bearing *N*,*N*′-chelating ligands: Synthesis, structures and *in vitro* cytotoxic studies on the A549 lung adenocarcinoma cell line

Lucie Melounková[a,b], Aneta Machálková[c], Radim Havelek[b], Jan Honzíček[c], Martina Řezáčová[b], Ivana Císařová[d], Eva Peterová[b,e], Jaromír Vinklárek[f,*]

[a] Department of Analytical Chemistry, Faculty of Chemical Technology, University of Pardubice, Studentská 573, 532 10 Pardubice, Czech Republic
[b] Department of Medical Biochemistry, Faculty of Medicine in Hradec Králové, Charles University, Šimkova 870, 500 38 Hradec Králové, Czech Republic
[c] Institute of Chemistry and Technology of Macromolecular Materials, Faculty of Chemical Technology, University of Pardubice, Studentská 573, 532 10 Pardubice, Czech Republic
[d] Department of Inorganic Chemistry, Faculty of Science, Charles University in Prague, Hlavova 2030/8, 128 43 Prague 2, Czech Republic
[e] 2nd Department of Internal Medicine - Gastroenterology, Charles University, Faculty of Medicine in Hradec Králové, University Hospital Hradec Králové, Czech Republic
[f] Department of General and Inorganic Chemistry, Faculty of Chemical Technology, University of Pardubice, Studentská 573, 532 10 Pardubice, Czech Republic

ARTICLE INFO

Keywords:
Vanadium(IV)
Cytotoxicity
Apoptosis
A549 lung adenocarcinoma cells

ABSTRACT

Ten new vanadocene complexes bearing *N*,*N*′-chelating ligands were prepared, characterized, and their cytotoxicity toward a panel of cancer cells was measured. Structures of four vanadocene compounds were determined by single crystal X-ray diffraction analysis. Complexes containing 1,2-bis(phenylimino)acenaphthene (bian) and 1,2-bis(4-methoxyphenylimino)acenaphthene (4-MeO-bian) exhibit higher cytotoxicity than those with dipyrido[3,2-*a*:2′,3′-*c*]phenazine (dppz) and (*E*)-*N*-((pyridin-2-yl)methylene)benzenamine (pyma). In light of the finding, cytotoxic mechanisms of two highly effective complexes $[(\eta^5\text{-}C_5H_4Me)_2V(bian)][OTf]_2$ (**3b**) and $[(\eta^5\text{-}C_5H_4Me)_2V(4\text{-}MeO\text{-}bian)][OTf]_2$ (**4b**) against human A549 lung adenocarcinoma cells were investigated by following membrane leakage of intracellular lactate dehydrogenase, Trypan Blue staining and activation of tumor protein p53 (p53). Evaluated complexes have a potent dose-dependent antiproliferative activity, causing cell cycle redistribution by the increased accumulation of cells in the G2 and S phase. In accord with the observed cell cycle deceleration, cyclin-dependent kinase inhibitor-interacting protein 1 ($p21^{WAF1/Cip1}$), extracellular signal–regulated kinases 1 and 2 (ERK1/2), Checkpoint kinase 1 (Chk1), Checkpoint kinase 2 (Chk2) and their phosphorylated forms Chk1 at serine 345 and Chk2 at threonine 68 increased. In the cells exposed to complexes, dose- and time-dependent apoptotic process is initiated by the activation of the initiator caspase 8, followed by activation of effector caspase 3/7 and phosphatidylserine externalization. Moreover, because of treatment, A549 cells activate prosurvival mitogen-activated protein kinases (MAPK) signaling and up-regulate antiapoptotic protein B-cell lymphoma (Bcl-2), thereby promoting evasion of cell death. Both complexes exhibited considerably higher cytotoxic effect than the reference anticancer drug *cis*-platin and the cytotoxicity was more pronounced at higher treatment time.

1. Introduction

Lung cancer is the second leading cause of death from cancer, causing more than one million deaths worldwide every year [1]. Adenocarcinoma represents the most common histological type of lung cancer [2], which belongs to the subgroup of the non-small cell lung cancer (NSCLC) [3]. Approximately 85% of lung cancers are NSCLC, and the diagnosis of NSCLC is associated with a worse prognosis in patients. For the successful treatment of NSCLC, chemical or radiation therapies after surgical excision have been identified as optimal treatment procedures. However, even if these treatment methods provide the desired outcome, only 15% of patients survive > 5 years because of frequent diagnosis in late stage, drug resistance and disease recurrence [4,5].

Several gene mutations that contribute to treatment resistance have been identified in lung adenocarcinomas [6]. Although most of the lung adenocarcinomas lack an identifiable driver oncogene that would contribute to aberrant proliferation and drug resistance, some

* Corresponding author at: Department of General and Inorganic Chemistry, Faculty of Chemical Technology, University of Pardubice, Studentská 573, 532 10 Pardubice, Czech Republic.
E-mail address: jaromir.vinklarek@upce.cz (J. Vinklárek).

https://doi.org/10.1016/j.jinorgbio.2019.03.015
Received 6 August 2018; Received in revised form 15 March 2019; Accepted 18 March 2019
Available online 22 March 2019
0162-0134/

abnormalities for suppression of tumor were identified, e.g. on tumor protein p53 (p53) [7]. Since genotoxic and cellular stress, signals for apoptosis-mediated cell death caused by DNA-targeting anticancer agents such as *cis*-platin go at least partly through p53 signaling, deficiency of p53 will attenuate its function and contributes to treatment resistance. In addition, the longer chemotherapy administrations continues, the stronger acquired resistance develops alongside treatment. Therefore, various efforts are ongoing to improve therapies with existing traditional chemotherapy drugs. In this regard, combined regimen using *cis*-platin in combination with other classical anticancer drugs showed several benefits over monotherapy. In addition, introduction of combination therapies and molecular-targeted drugs like Gefitinib showed improved overall survival in NSCLC treatment [8]. On the other hand, even many newer, high-dose chemotherapy or drug combination therapies increase a risk of adverse side effects, making the treatment burdensome and less suitable for physically weakened patients with more advanced stages of NSCLC. While response rates to combination therapies may be higher, the median overall survival for patients with NSCLC is still limited [9]. Therefore, even if treatment of NSCLC with genotoxic chemotherapeutic have provided the standard regimens backbone in terms of efficacy, a quest for specific and effective chemotherapeutic agents for NSCLC is still ongoing [10].

Recently, vanadium complexes containing stabilizing by *N*,*N*′-chelating ligands got into foreground of interest in a human in vitro model of NSCLC due to visible light-induced photocytotoxicity in lung carcinoma A549 cells with half-maximal inhibitory concentration (IC_{50}) of 17 μM [11]. Vanadocene dichloride $[(\eta^5\text{-}C_5H_5)_2VCl_2]$ (**1a**) is known as potent antitumor agent with low general toxicity [12–15]. Our recent studies have demonstrated that substitution of chloride ligands [16,17] as well as modification of the cyclopentadienyl rings (Cp) [12] considerably changes physicochemical properties of the complex species and can lead to the highly cytotoxic agents. For example, the vanadocene complex $[(\eta^5\text{-}C_5H_5)_2V(5\text{-}NH_2\text{-phen})][OTf]_2$ bearing substituted 1,10-phenanthroline (phen) is about twenty times more active toward leukemic cells MOLT-4 than parent dichloride species **1a**, which was ascribed to the higher stability in aqueous media [18].

Additionally, the literature describes a pharmacological potential of vanadium connected with treatment of diabetes mellitus and potential mimic of insulin signaling by peroral application of sodium metavanadate and vanadyl sulfate [19,20]. The vanadium (IV) compound with vitamin A $[VO(\text{vitamin A})_2(H_2O)_2]$ was proven as an antidiabetic agent, which interferes with lipid profile and antioxidant activity (increase of superoxide dismutase, malondialdehyde, glutathione) [21]. Also vanadium(IV) chelates were studied for their ability to reduce hyperglycemia with encouraging results [22,23]. It was found out that the vanadium(IV) has inhibition effect on the glyceraldehyde 3-phosphate dehydrogenase, lipoprotein lipase, protein tyrosine phosphatases, glucose-6-phosphate dehydrogenase, glycogen synthase, adenylate cyclase and cytochrome oxidase. On the contrary, the vanadium(IV) stimulates the following functions: Na^+/K^+–ATPase, H^+/K^+–ATPase, myosin ATPase, adenylate kinase, phosphofructokinase and cholinesterase. Thanks to these effects, it can be used as agent with antihyperlipidemic effect, antiobesitic effect, with antihypertensive properties and diuretic effect [19,20]. Beside other things, the vanadium compounds inhibit the epithelial-mesenchymal transition [24]. However, the primary effect of the vanadium is activation of the apoptotic path in cancer cells [25].

The aim of this study is to determine cytotoxic effect of new vanadocene complexes bearing *N*,*N*′-chelating ligands. After an initial cytotoxicity screening, highly effective complexes $[(\eta^5\text{-}C_5H_4Me)_2V(\text{bian})][OTf]_2$ (bian = 1,2-bis(phenylimino)acenaphthene) (**3b**) and $[(\eta^5\text{-}C_5H_4Me)_2V(\text{4-MeO-bian})][OTf]_2$ (4-MeO-bian = 1,2-bis(4-methoxyphenylimino)acenaphthene) (**4b**), which showed impressive activity against A549 lung adenocarcinoma cells, were chosen for study on exploring the mechanism of cytotoxic activity. The experiments are focused on evaluation of the cell membrane integrity using the Trypan Blue dye exclusion, quantification of apoptotic process induction using flow cytometry analysis of Annexin V binding and through evaluation of caspases activity. The expression of cell proteins with cardinal impact on cell cycle progression is determined by Western blots analysis combined with sodium dodecyl sulfate–polyacrylamide gel electrophoresis and immunochemical detection.

2. Methods and materials

2.1. Synthesis of the complexes

All operations were performed under nitrogen using conventional Schlenk-line techniques. The solvents were purified and deoxygenated by standard methods [26]. $[(\eta^5\text{-}C_5H_5)_2VCl_2]$ (**1a**) [27] $[(\eta^5\text{-}C_5H_4Me)_2VCl_2]$ (**1b**) [28], dipyrido[3,2-*a*:2′,3′-*c*]phenazine (dppz) [29] (*E*)-*N*-((pyridin-2-yl)methylene)benzenamine (pyma) [29], bian [30] and 4-MeO-bian [30] were prepared according literature procedures. Benzene-1,2-diamine (bda) and silver trifluoromethanesulfonate (AgOTf) were obtained from Sigma-Aldrich and used without further purification.

Infrared spectra were recorded on a Nicolet iS50 FTIR spectrometer in the 4000–400 cm^{-1} region using attenuated total reflectance technique. The electron paramagnetic resonance (EPR) spectra were recorded on a Miniscope MS 300 spectrometer at X-band at ambient temperature. Mass spectrometry (MS) was performed on a LCMS 2010 quadrupole mass spectrometer quadrupole mass spectrometer (Shimadzu, Japan). The sample was injected into the mass spectrometer with infusion mode at a constant flow rate of 10 L/min, and electrospray ionization mass spectrometry was used for identification of analyzed samples.

2.1.1. Synthesis of $[(\eta^5\text{-}C_5H_5)_2V(\text{bian})][OTf]_2$ (3a)

$[(\eta^5\text{-}C_5H_5)_2VCl_2]$ (**1a**; 0.252 g, 1.00 mmol) was dissolved in tetrahydrofuran (THF) (20 mL), treated with AgOTf (0.514 g, 2.00 mmol) and stirred for 90 min in darkness. The reaction mixture was filtered through a short pad of Celite to remove a fine precipitate of silver chloride. The clear green solution was treated with bian (0.499 g, 1.50 mmol) that causes immediate color change from green to brown. The reaction mixture was stirred for 24 h. The solid product was separated by decantation. It was washed with THF and ether and dried under vacuum. Yield: 0.219 g (27%, 0.27 mmol). Brown powder. Calc. for $C_{36}H_{26}F_6N_2O_6S_2V$ (MW 811.67): C, 53.27; H, 3.23; N, 3.45; S, 7.90. Anal. Found: C, 53.25; H, 3.24; N, 3.42; S, 7.88. Positive ion MS (MeOH): m/z = 256.4 $[M]^{2+}$. EPR(MeOH): $|A_{iso}|$ = 68.8 G, g_{iso} = 1.982. IR(ATR, cm^{-1}): 3105w, 1715w, 1619w, 1581m, 1486w, 1449w, 1431w, 1259vs, 1221s, 1154s, 1021vs, 859m, 831m, 765s, 698s, 632vs, 571m, 544m, 518s.

2.1.2. Synthesis of $[(\eta^5\text{-}C_5H_4Me)_2V(\text{bian})][OTf]_2$ (3b)

The reaction was carried out as described for **3a** but with $[(\eta^5\text{-}C_5H_4Me)_2VCl_2]$ (**1b**; 0.280 g, 1.00 mmol), AgOTf (0.514 g, 2.00 mmol) and bian (0.499 g, 1.50 mmol). Brown powder. Yield: 0.193 g (23%, 0.23 mmol). Calc. for $C_{38}H_{30}F_6N_2O_6S_2V$ (MW 839.72): C, 54.35; H, 3.60; N, 3.34; S, 7.64. Anal. Found: C, 54.36; H, 3.58; N, 3.30; S, 7.60. Positive ion MS(MeOH): m/z = 270.5 $[M]^{2+}$. EPR(MeOH): $|A_{iso}|$ = 68.7 G, g_{iso} = 1.982. IR(ATR, cm^{-1}): 3121w, 1610w, 1581w, 1486w, 1440w, 1259vs, 1154s, 1030vs, 1021vs, 831s, 774s, 632vs, 575m, 546m, 518s.

2.1.3. Synthesis of $[(\eta^5\text{-}C_5H_5)_2V(\text{4-MeO-bian})][OTf]_2$ (4a)

The reaction was carried out as described for **3a** but with $[(\eta^5\text{-}C_5H_5)_2VCl_2]$ (**1a**; 0.252 g, 1.00 mmol), AgOTf (0.514 g, 2.00 mmol) and 4-MeO-bian (0.589 g, 1.50 mmol). Orange powder. Yield: 0.227 g (26%, 0.26 mmol). Calc. for $C_{38}H_{30}F_6N_2O_8S_2V$ (MW 871.72): C, 52.36; H, 3.47; N, 3.21; S, 7.36. Anal. Found: C, 52.35; H, 3.50; N, 3.20; S, 7.33. Positive ion MS(MeOH): m/z = 286.5 $[M]^{2+}$. EPR(MeOH):

$|A_{iso}|$ = 68.4 G; g_{iso} = 1.984. IR(ATR, cm^{-1}): 3118w, 1599w, 1559w, 1510m, 1436w, 1249vs, 1151s, 1028vs, 857m, 832s, 775s, 726w, 702w, 636vs, 571m, 546m, 539m 514s, 416w. Single crystals of **4a** suitable for X-ray diffraction analysis were prepared by careful overlayering of acetonitrile solution with ether.

2.1.4. Synthesis of [(η^5-$C_5H_4Me)_2V(4$-MeO-bian)][OTf]$_2$ (4b)

The reaction was carried out as described for **3a** but with [(η^5-$C_5H_4Me)_2VCl_2$] (**1b**; 0.280 g, 1.00 mmol), AgOTf (0.514 g, 2.00 mmol) and 4-MeO-bian (0.589 g, 1.50 mmol). Yield: 0.270 g (30%, 0.30 mmol). Orange powder. Calc. for $C_{40}H_{34}F_6N_2O_8S_2V$ (MW 899.77): C, 53.40; H, 3.81; N, 3.11; S, 7.13. Anal. Found: C, 53.41; H, 3.8; N, 3.10; S, 7.12. Positive ion MS(MeOH): m/z = 300.5 $[M]^{2+}$. EPR (MeOH): $|A_{iso}|$ = 68.4 G, g_{iso} = 1.984. IR(ATR, cm^{-1}): 3114w, 2960w, 2833w, 1603w, 1504m, 1458w, 1440w, 1250vs, 1141s, 1033vs, 834s, 780s, 725w, 635vs, 571m, 536w, 518s.

2.1.5. Synthesis of [(η^5-$C_5H_5)_2V(pyma)$][OTf]$_2$ (5a)

The reaction was carried out as described for **3a** but with [(η^5-$C_5H_5)_2VCl_2$] (**1a**; 0.252 g, 1.00 mmol), AgOTf (0.514 g, 2.00 mmol) and pyma (0.273 g, 1.50 mmol). Dark brown powder. Yield: 0.137 g (18%, 0.18 mmol). Dark brown powder. Calc. for $C_{30}H_{20}F_6N_4O_6S_2V$ (MW 761.57): C, 47.31; H, 2.65; N, 7.36; S, 8.42. Anal. Found: C, 47.30; H, 2.63; N, 7.34; S, 8.43. Positive ion MS(MeOH): m/z = 181.5 $[M]^{2+}$. EPR(MeOH): $|A_{iso}|$ = 67.8 G; g_{iso} = 1.986. IR(ATR, cm^{-1}): 3111w, 1593w, 1585w, 1494w, 1440w, 1431w, 1250vs, 1222s, 1151s, 1024vs, 861s, 852s, 770m, 698m, 635vs, 571s, 518s. Single crystals of **5a** suitable for X-ray diffraction analysis were prepared by careful overlayering of the acetonitrile solution with ether.

2.1.6. Synthesis of [(η^5-$C_5H_4Me)_2V(pyma)$][OTf]$_2$ (5b)

The reaction was carried out as described for **3a** but with [(η^5-$C_5H_4Me)_2VCl_2$] (**1b**; 0.280 g, 1.00 mmol), AgOTf (0.514 g, 2.00 mmol) and pyma (0.273 g, 1.50 mmol). Yield: 0.150 g (19%, 0.19 mmol). Dark brown powder. Calc. for $C_{32}H_{24}F_6N_4O_6S_2V$ (MW 789.62): C, 48.67; H, 3.06; N, 7.10; S, 8.12. Anal. Found: C, 48.66; H, 3.05; N, 7.12; S, 8.10. Positive ion MS(MeOH): m/z = 195.6 $[M]^{2+}$. EPR(MeOH): $|A_{iso}|$ = 67.8 G; g_{iso} = 1.986. IR(ATR, cm^{-1}): 3086w, 1593w, 1494m, 1449w, 1250vs, 1241vs, 1151s, 1024vs, 960w, 870m, 780m, 743m, 698m, 635vs, 626vs, 571s, 518s.

2.1.7. Synthesis of [(η^5-$C_5H_5)_2V(dppz)$][OTf]$_2$ (6a)

The reaction was carried out as described for **3a** but with [(η^5-$C_5H_5)_2VCl_2$] (**1a**; 0.252 g, 1.00 mmol), AgOTf (0.514 g, 2.00 mmol) and dppz (0.423 g, 1.50 mmol). Yield: 0.146 g (22%, 0.22 mmol). Grey powder. Calc. for $C_{24}H_{20}F_6N_2O_6S_2V$ (MW 661.49): C, 43.58; H, 3.05; N, 4.23; S, 9.70. Anal. Found: C, 43.55; H, 3.08; N, 4.25; S, 9.73. Positive ion MS(MeOH): m/z = 231.6 $[M]^{2+}$. EPR(MeOH): $|A_{iso}|$ = 67.2 G; g_{iso} = 1.986. IR(ATR, cm^{-1}): 3096w, 1619w, 1505w, 1430w, 1354w, 1268vs, 1259vs, 1222s, 1151s, 1078m, 1033vs, 1024vs, 869m, 831m, 770m, 765s, 727s, 635vs, 626s, 575s, 518s, 470w, 432m, 403m. Single crystals of **6a**·MeCN suitable for X-ray diffraction analysis were prepared by careful overlayering of the acetonitrile solution with ether.

2.1.8. Synthesis of [(η^5-$C_5H_4Me)_2V(dppz)$][OTf]$_2$ (6b)

The reaction was carried out as described for **3a** but with [(η^5-$C_5H_4Me)_2VCl_2$] (**1b**; 0.280 g, 1.00 mmol), AgOTf (0.514 g, 2.00 mmol) and dppz (0.423 g, 1.5 mmol). Yield: 0.138 g (20%, 0.20 mmol). Grey powder. Calc. for $C_{26}H_{24}F_6N_2O_6S_2V$ (MW 689.54): C, 45.29; H, 3.51; N, 4.06; S, 9.30. Anal. Found: C, 45.30; H, 3.50; N, 4.06; S, 9.28. Positive ion MS(MeOH): m/z = 245.5 $[M]^{2+}$. EPR(MeOH): $|A_{iso}|$ = 67.2 G; g_{iso} = 1.986. IR(ATR, cm^{-1}): 3083w, 1619w, 1496w, 1430w, 1354w, 1268vs, 1259vs, 1221s, 1164s, 1078m, 1030vs, 1021vs, 888w, 812m, 765m, 727s, 632vs, 622s, 575s, 518s, 460w, 432m, 413m.

2.1.9. Synthesis of [(η^5-$C_5H_5)_2V(bda)$][OTf]$_2$ (7a)

The reaction was carried out as described for **3a** but with [(η^5-$C_5H_5)_2VCl_2$] (**1a**; 0.252 g, 1.00 mmol), AgOTf (0.514 g, 2.00 mmol) and dba (0.162 g, 1.50 mmol). Yield: 0.182 g (31%, 0.31 mmol). Grey powder. Calc. for $C_{18}H_{18}F_6N_2O_6S_2V$ (MW 587.41): C, 36.80; H, 3.09; N, 4.77; S, 10.92. Anal. Found: C, 36.82; H, 3.10; N, 4.74; S, 10.88. Positive ion MS(MeOH): m/z = 144.5 $[M]^{2+}$. EPR(MeOH): $|A_{iso}|$ = 68.0 G; g_{iso} = 1.984. IR(ATR, cm^{-1}): 3178w, 3111m, 1610w, 1496w, 1449w, 1440w, 1278s, 1249vs, 1221vs, 1164s, 1154s, 1097w, 1030vs, 1021vs, 878m, 869m, 850m, 765m, 632vs, 622vs, 575s, 518s, 441w, 403w. Single crystals of **7a** suitable for X-ray diffraction analysis were prepared by careful overlayering of the acetonitrile solution of with ether.

2.1.10. Synthesis of [(η^5-$C_5H_4Me)_2V(bda)$][OTf]$_2$ (7b)

The reaction was carried out as described for **3a** but with [(η^5-$C_5H_4Me)_2VCl_2$] (**1b**; 0.280 g, 1 mmol), AgOTf (0.514 g, 2.00 mmol) and dba (0.162 g, 1.5 mmol). Yield: 0.209 g (34%, 0.34 mmol). Grey powder. Calc. for $C_{20}H_{22}F_6N_2O_6S_2V$ (MW 615.46): C, 39.03; H, 3.60; N, 4.55; S, 10.42. Anal. Found: C, 39.00; H, 3.58; N, 4.53; S, 10.40%. Positive ion MS(MeOH): m/z = 158.5 $[M]^{2+}$. EPR(MeOH): $|A_{iso}|$ = 67.9 G; g_{iso} = 1.984. IR(ATR, cm^{-1}): 3178w, 3111m, 1610w, 1496m, 1459w, 1392w, 1278s, 1240s, 1230vs, 1221vs, 1164s, 1154s, 1030s, 1021s, 878m, 765m, 755m, 632s, 622s, 575s, 518s, 441m, 432m, 403w.

2.2. X-ray crystallography

Crystallographic data were collected on Bruker D8 VENTURE Kappa Duo PHOTON100 by IμS micro-focus sealed tube MoKα radiation (λ = 0.71073 Å) at the temperature 150 K. The structures were solved by direct methods (XT) [31] and refined by full matrix least squares based on F^2 (SHELXL2014) [32]. The hydrogen atoms on carbon were fixed into idealized positions (riding model) and assigned temperature factors either $H_{iso}(H)$ = 1.2 U_{eq} (pivot atom) or $H_{iso}(H)$ = 1.5 U_{eq} (pivot atom) for methyl moiety. The unit cell of complex **5a** includes two crystallographically independent but essentially identical molecules. CCDC 1565048 (for **4a**), 1565049 (for **6a**·MeCN), 1565050 (for **5a**) and 1565051 (for **7a**) contain the supplementary crystallographic data for this paper. These data can be obtained free of charge from The Cambridge Crystallographic Data Centre.

2.3. Cell line and culture conditions

For our experiments, non-small human lung alveolar carcinoma epithelial A549 cells from the European Collection of Cell Cultures (UK) were used. The A549 cells were cultured in the Dulbecco's Modified Eagle's medium supplemented with 10% fetal bovine serum, 0.05% L-glutamine, 150 μg/mL penicillin and 50 μg/mL streptomycin (all reagents from Sigma-Aldrich, USA). The cell line was cultured at 37 °C in a humidified atmosphere with 5% CO_2. Each two days the cultures were diluted to a concentration of 2 × 10^5 cells/mL. The A549 cells in the maximal range of up to 20 passages were used for this study.

2.4. Preparation of solution of the test compounds

Stock solutions were prepared by dissolving all complexes in absolute ethanol (EtOH). The test complexes were dissolved in 1 mL of the culture medium and EtOH in total volume lower than 0.5% w/v. For the experiments, the stock solutions of **3b** and **4b** were diluted with the complete culture medium for A549 cells to create final concentrations, making sure the concentration of EtOH was < 0.5% w/v to avoid toxic effects on cells. Notably, EtOH in concentration 0.5% w/v did not exhibit any significant negative effect on cell proliferation during cytotoxicity screening within 24 and 48 h of application (decrease in growth percentage as compared to untreated control cells) (Fig. S1 in the Supporting information).

2.5. Primary screening of cytotoxicity

Selected human tumor cell lines (A2780 - ovarian adenocarcinoma, A549 - lung adenocarcinoma, Saos2 - osteogenic sarcoma, HeLa - colon adenocarcinoma, HT-29 - colon adenocarcinoma, Jurkat - leukemic T cell lymphoblast, MCF-7 - breast adenocarcinoma, MOLT-4 - leukemic lymphoblastoid, PANC-1 - pancreatic carcinoma of ductal origin) were purchased from either ATCC, USA or Sigma-Aldrich, USA and cultured according to the provider's culture method guidelines. All cell lines were maintained at 37 °C in a humidified 5% carbon dioxide and 95% air incubator. For initial screening of cytotoxicity, the cells were seeded at appropriate, a previously established optimal density in 96-well plates and allowed to settle overnight. Cells were treated by **3a–7b** for 48 h. Final concentration of derivatives was 10 μM. At the end of cultivation, WST-1 proliferation assay (Roche Applied Science, Switzerland) was performed according to the manufacturer's instructions and the absorbance was measured using Tecan Infinite M200 (Tecan Group, Switzerland). Cytotoxicity assay is based on a reduction of 2-(4-iodophenyl)-3-(4-nitrophenyl)-5-(2,4-disulfophenyl)-*2H*-tetrazolium sodium salt (WST-1) to a water-soluble formazan by viable cells. For primary screening, each value is the mean of absorbance measured in four wells and represents the percentage of negative control, non-treated cells (100%). Three independent experiments were performed; results are expressed as mean ± standard deviation (SD).

2.6. Determination of cytotoxicity over the concentration range

Cell viability was quantified using the colorimetric WST-1 Cell Proliferation Reagent (Roche Applied Science, Switzerland). The A549 cells were seeded at a concentration 500 cells/well for 24 h interval, 350 cells/well for 48 h interval in 100 μL of culture medium and cells were allowed to reattach overnight. Thereafter, the cells were treated with 100 μL of corresponding **3b**, **4b** and *cis*-platin stock solutions to obtain the desired concentrations of 0.1, 0.3, 0.7, 1.5, 2.5, 4, 9, 15, 27, 50 μM in total volume of 200 μL. The sample set was incubated for 24 h or 48 h at 37 °C in a humidified atmosphere with 5% CO_2. After incubation time, 50 μL of WST-1 solution was added to each well. Following 3 h of incubation, the absorbance at 440 nm was measured using multiple reader Tecan Infinite M200 (Tecan Group, Switzerland). Cytotoxicity was evaluated as 50% inhibition concentration (IC_{50}) value using the statistic software Origin Pro (version 9, OriginLabCorporation, USA). Three independent experiments were performed; results are expressed as mean ± SD.

2.7. Proliferation assay

Cell membrane integrity was determined microscopically using 0.5% Trypan blue water solution (Sigma-Aldrich, USA). The cells affected by cytotoxic agents are stained blue in microscope. Cell proliferation of unstained cells was evaluated 24 h after the treatment of 1×10^6 A549 cells with 1, 3, 5, 10 μM of **3b** and **4b** complexes. As a control, 1×10^6 of non-treated A549 cells were used. Cell counting was carried out in Bürker chamber. Three independent experiments were performed; results are expressed as mean ± SD.

2.8. LDH leakage

Activity of lactate dehydrogenase (LDH) activity was determined at 24 and 48 h in the cultivation medium (with max 1% fetal bovine serum) of A549 cells exposed with 1, 2, 4 and 6 μM of **3b**, **4b** and *cis*-platin (10, 20, 40 and 60 μM for 24 h resp. 5, 10, 20, 40 μM for 48 h) using a commercially available kit (Roche Applied Science, Switzerland). Non-treated A549 cells were used as a control. The total LDH activity was determined after sonication of the cells. The enzyme activity was determined spectrophotometrically using multiple reader Tecan Infinite M200 (Tecan Group, Switzerland) and the rate of enzyme leakage was expressed as percentage of the total LDH activity compared to untreated control cells. Three independent experiments were performed; results are expressed as mean ± SD.

2.9. Determination of apoptosis

Apoptest-FITC (FITC = fluorescein isothiocyanate) kit (Dako-Cytomation, Denmark) was used for determination of apoptosis. One of the earliest indicator of cells undergoing apoptosis is translocation of phosphatidylserine to the outer layer of cell membrane. The Annexin V protein conjugated to a FITC has high affinity (in the presence of calcium ions) to the phosphatidylserine. During the stages of late apoptosis and necrosis, when cell membrane becomes permeable, propidium iodide enters the cell and binds to DNA. The A549 cells in the amount 1×10^6 cells/5 mL medium were treated in concentrations 1, 2, 4 and 6 μM of the complex **3b** and 0.5, 1, 2, 4 μM of **4b**. *cis*-Platin was used in concentrations 10, 20, 40, 60 μM for the incubation time 24 h and 5, 10, 20, 40 μM for the incubation time 48 h. Non-treated A549 cells were used as a control. For each condition, the samples were analyzed by the flow cytometer CyAn ADP (Beckman Coulter, USA). Listmode data were analyzed using the Kaluza Analysis 1.3 software (Beckman Coulter, USA). Three independent experiments were performed; results are expressed as mean ± SD.

2.10. Activity of caspases

Programmed cell death was determined by measuring the activity of caspases 3/7, 8 and 9 using the Caspase-Glo Assays (Promega, USA) 24 h after the treatment of A549 cells. Concentrations of the test complexes were 1, 2 and 4 μM for **3b** and **4b**. Non-treated A549 cells and the cells treated with *cis*-platin (40 μM) were used a negative and positive control, respectively. Briefly, 1×10^4 of the cells was seeded per well using a 96-well-plate format (Sigma-Aldrich, USA). After addition of 50 μL of Caspase-Glo reagents into each well of microplate, caspase cleavage of the substrate followed. This generated a luminescent signal. The incubation lasted 30 min at 37 °C in a humidified atmosphere with 5% CO_2. Luminescence was measured using a multiple reader Tecan Infinite M200 (Tecan Group, Switzerland). Three independent experiments were performed; results are expressed as mean ± SD.

2.11. Determination of cell cycle distributions

Cell cycle was analyzed using flow cytometry in A549 cells following 24 and 48 h of treatment with 1, 2, 4 and 6 μM of **3b** and 0.5, 1, 2, 4 μM of **4b**. *cis*-Platin was used in the concentration 10, 20, 40, 60 μM for the incubation time 24 h and 5, 10, 20, 40 μM for the incubation time 48 h. In each experiment, the cells were washed with cold phosphate buffered saline sterile and fixed with 70% EtOH. For detection of low molecular-weight fragments of DNA, the cells were incubated for 5 min. at room temperature in a buffer (192 mL 0.2 mol/L Na_2HPO_4 + 8 mL of 0.1 mol/L citric acid, pH 7.8) and then labelled with propidium iodide in Vindelov's solution for 1 h at 37 °C. The DNA content was determined by the flow cytometer CyAn ADP (Beckman Coulter, USA). Data were analyzed using the Multicycle AV software (Phoenix Flow systems, USA). All reagents were obtained from Sigma-Aldrich, USA. Three independent experiments were performed; results are expressed as mean ± SD.

2.12. Electrophoresis and analysis by Western blots

A549 cells were pre-incubated with the test compounds at increasing concentrations 1, 2, 4 μM of **3b** and **4b**. As a negative control, non-treated A549 cells were used. *cis*-Platin in concentration of 40 μM was used as a positive control. Two treatment periods were chosen (4 and 24 h) for the determination of complexes activity. Thereafter, whole cell lysates were prepared. The total amount of protein was

determined using the bicinchoninic acid assay (Sigma-Aldrich, USA). Equivalent amount (30 μg) of protein from each lysate was loaded into lanes of 12% sodium dodecyl sulfate-polyacrylamide gel. After electrophoretic separation, the proteins were transferred onto a polyvinylidene difluoride membrane (Bio-Rad Laboratories, France). Non-specific binding of the membranes was blocked by application of Tris-buffered saline containing 0.05% Tween 20 and 10% non-fat dry milk. Incubation with primary monoclonal antibody was performed overnight at 4 °C. After washing, the membranes were incubated with secondary polyclonal antibody for 1 h at room temperature. For the signal detection a chemiluminescent detection kit (Roche, Czech Republic) was using the PXi imaging system (Syngene, Cambridge UK). To ensure equal protein loading, each membrane was reprobed and β-actin was detected.

2.13. Statistical analysis

The cytotoxicity determination of results using WST-1 were expressed as mean ± SD of three independent experiments. By software Origin Pro (version 8, Microcal Software, Inc. Northamptom, MA, USA), in the block "Analyses" by statistical method "ANOVA" the graph of viability of cells depending on the concentration of the test complexes was constructed.

For all other experiments, statistics were calculated and the charts were made in the Microsoft Office Excel 2003 (Microsoft Inc., Redmond, WA, USA). In this study, all the values were expressed as arithmetic means with standard deviation. The statistical analysis of differences between the groups was performed by the Student's *t*-test and P values ≤0.05 were considered significant.

3. Results

3.1. Preparation and characterization of the test complexes

Vanadocene and 1,1′-dimethylvanadocene compounds bearing *N,N′*-chelating ligands $[(\eta^5\text{-}C_5H_5R)_2V(^{N,N}L)][OTf]_2$ (**3a**: R = H, ^{N,N}L = bian; **3b**: R = Me, ^{N,N}L = bian; **4a**: R = H, ^{N,N}L = 4-MeO-bian; **4b**: R = Me, ^{N,N}L = 4-MeO-bian; **5a**: R = H, ^{N,N}L = pyma; **5b**: R = Me, ^{N,N}L = pyma; **6a**: R = H, ^{N,N}L = dppz; **6b**: R = Me, ^{N,N}L = dppz; **7a**: R = H, ^{N,N}L = bda; **7b**: R = Me, ^{N,N}L = bda) were prepared from chloride analogues according to Scheme 1.

In the first step, chloride ligands are exchanged by triflates to give $[(\eta^5\text{-}C_5H_4R)_2V(OTf)_2]$ (**2a**: R = H; **2b**: Me). The reaction is driven by precipitation of silver chloride. In the second reaction step, weakly coordinated triflate ligands are exchanged with *N,N′*-chelating ligand to give appropriate dicationic vanadocene complexes. The synthesized complexes (**3a–7a** and **3b–7b**) were isolated and characterized by elemental analysis, mass spectrometry, infrared and EPR spectroscopy. We note that all synthesized compounds were air-stable for days. Nevertheless, long-term storage was done under inert atmosphere of nitrogen.

The assembly of dicationic species $[(\eta^5\text{-}C_5H_4R)_2V(^{N,N}L)]^{2+}$ was evidenced in first-order positive-ion ESI mass spectra. All compounds under the study (**3a–7a** and **3b–7b**) appear as base peaks. The infrared spectra of the complexes show expected vibration modes of the aliphatic [ν(C–H) ~2920 cm^{-1}] as well as the aromatic parts [ν_a(C–H) ~3120 cm^{-1}; ν_s(C–H) ~3100 cm^{-1}; ν(C=C), ν(C=N) ~1580–1430 cm^{-1}] of the coordinated ligands.

Paramagnetic character of the compounds **3a–7a** and **3b–7b** enables to follow the coordination sphere of vanadium by EPR spectroscopy. The complexes give EPR spectra with strong hyperfine coupling (HFC) appearing due to interaction of the unpaired electron with the nuclear spin of ^{51}V ($I = {}^7/_2$, 99.8%). The coordination of chelating ligand is evident from low values of isotropic HFC constant (**3a–7a**: $|A_{iso}|$ = 67.2–68.8 G and **3b–7b**: $|A_{iso}|$ = 67.2–68.7 G), which reveals considerably higher delocalization of unpaired electron than in the case of starting dichlorides (**1a** and **1b**) and triflate intermediates (**2a** and **2b**) [18]. The observed $|A_{iso}|$ and g_{iso} values, given in Table 1, well correlate with data previously reported vanadocene compounds bearing another series of *N,N′*-chelating ligands [17,18,33]. The effect of substitution in cyclopentadienyl ring on the EPR parameters is negligible.

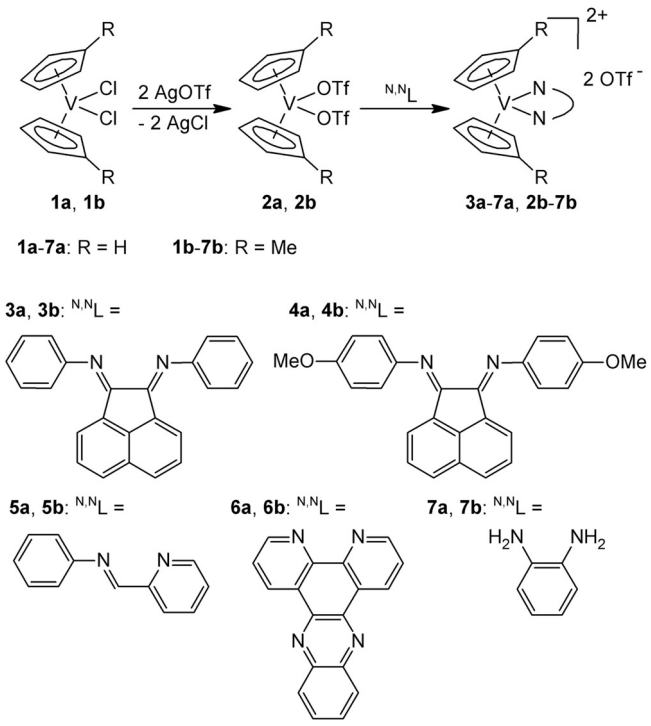

Scheme 1. Preparation of vanadocene complexes bearing *N,N′*-chelating ligands.

Table 1
Isotropic g-factors and isotropic HFC constants (G) of the vanadocene complexes.

	$\lvert A_{iso}\rvert$	g_{iso}		$\lvert A_{iso}\rvert$	g_{iso}
3a	68.8	1.982	**3b**	68.7	1.982
4a	68.4	1.984	**4b**	68.4	1.984
5a	67.8	1.986	**5b**	67.8	1.986
6a	67.2	1.986	**6b**	67.2	1.986
7a	68.0	1.984	**7b**	67.9	1.984

The crystal structures of the compounds **4a**, **5a**, **6a**·MeCN and **7a** were determined by single crystal X-ray diffraction analysis. Molecular structures of the compounds are shown in Figs. 1–4. Important structural parameters are listed in Table 2. The dicationic complex species have a typical bend metallocene structure, in which two η^5-bonded cyclopentadienyl rings and two nitrogen donor atoms of the *N,N′*-chelating ligand occupy pseudotetrahedral coordination sites around the vanadium atom in the formal oxidation state IV. Distances between the centroid of the cyclopentadienyl ring and vanadium atom [Cg–V = 1.951(2)–1.9649(8) Å] as well as the Cg–V–Cg angles [133.36(4)–134.77(8)°] are in the range common for the previously reported vanadocene(IV) complexes [34]. The V–N bond lengths and the N–V–N bond angles of the complexes **4a**, **5a**, **6a**·MeCN and **7a** were found to be in the ranges 2.123(3)–2.1667(15) Å and 75.95(6)–76.90(4)°, respectively. The observed values are in good agreement with data reported for related compounds [17,18,33].

In compounds **4a**, **5a** and **6a**·MeCN, central metal stays very close to a plane of aromatic core of the ligand as evident from a small slip angle of the chelate ring [**4a**: 0.54(9)°, **5a**: 1.44(18)°, 3.40(18)°, **6a**·MeCN:

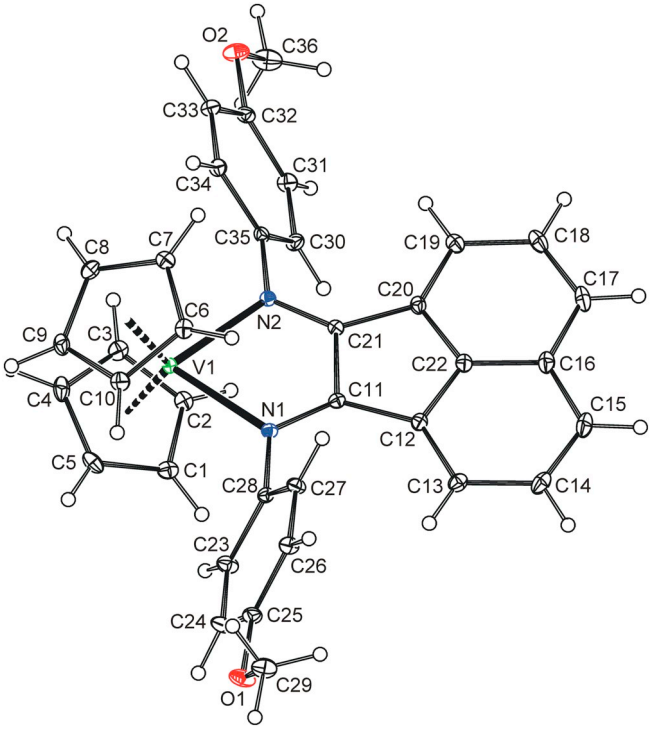

Fig. 1. ORTEP drawing of the dicationic complex $[(\eta^5\text{-}C_5H_5)_2V(4\text{-MeO-bian})]^{2+}$ present in the crystal structure of **4a** (ellipsoids: 30% probability). Numbering of all non-hydrogen atoms is shown.

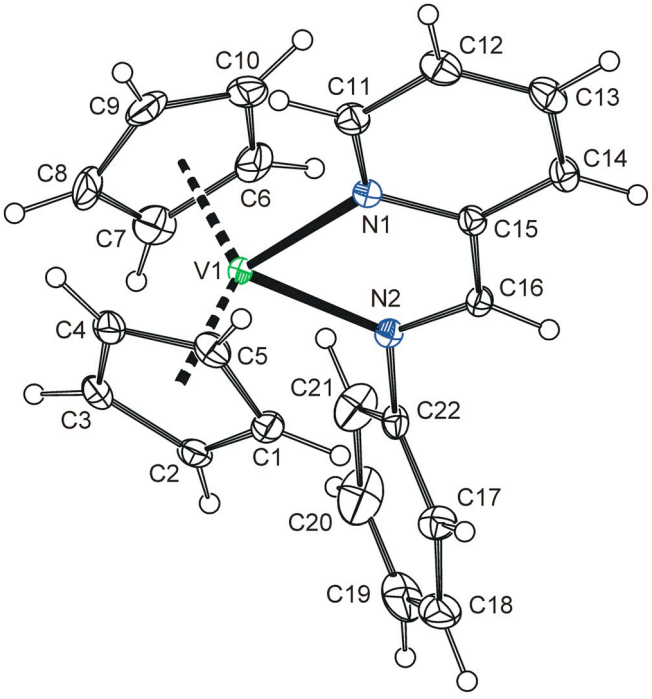

Fig. 2. ORTEP drawing of the dicationic complex $[(\eta^5\text{-}C_5H_5)_2V(pyma)]^{2+}$ present in the crystal structure of **5a** (ellipsoids: 30% probability). Numbering of all non-hydrogen atoms is shown.

6.89(16)°]. Such observation is in line with expected sp^2-hybridization of nitrogen donor atoms. Compound **7a** shows considerably larger slip angle of the chelate ring [31.65(10)°] due to coordination of sp^3-nitrogen atoms. We note that hybridization of nitrogen donor atoms has only minor effect on the V–N bond lengths and the N–V–N bond angles.

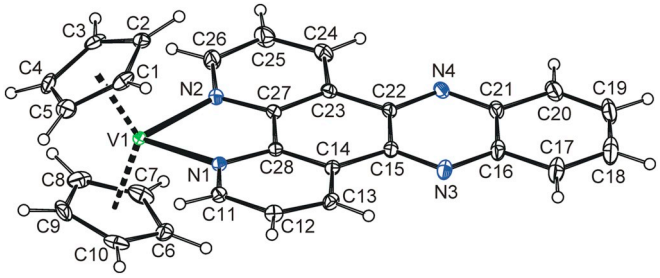

Fig. 3. ORTEP drawing of the dicationic complex $[(\eta^5\text{-}C_5H_5)_2V(dppz)]^{2+}$ present in the crystal structure of **6a** (ellipsoids: 30% probability). Numbering of all non-hydrogen atoms is shown.

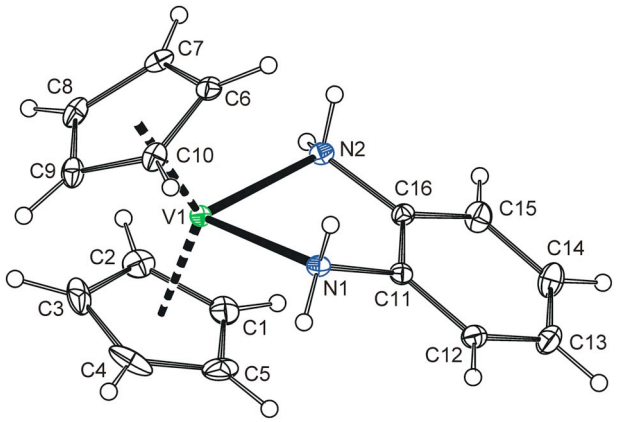

Fig. 4. ORTEP drawing of the dicationic complex $[(\eta^5\text{-}C_5H_5)_2V(bda)]^{2+}$ present in the crystal structure of **7a** (ellipsoids: 30% probability). Numbering of all non-hydrogen atoms is shown.

Table 2
Selected bond lengths (Å) and bond angles (°) for the compounds **4a–7a**.

	Cg–V[a]	V–N	Cg–V–Cg[a]	N–V–N
4a	1.9600(8)	2.1438(11)	133.88(3)	76.90(4)
	1.9649(8)	2.1520(12)		
5a[b]	1.951(2)	2.123(3)	133.96(8)	76.24(10)
	1.9531(17)	2.127(2)		
5a[b]	1.9510(16)	2.123(3)	134.77(8)	76.29(10)
	1.960(2)	2.134(2)		
6a	1.9499(15)	2.134(2)	134.19(7)	76.25(9)
	1.9558(14)	2.135(2)		
7a	1.9512(8)	2.1554(15)	133.36(4)	75.95(6)
	1.9610(10)	2.1667(15)		

[a] Cg is centroid of cyclopentadienyl ring.
[b] Two crystallographically independent molecules in the unit cells.

3.2. Cytotoxicity assay

Cytotoxicity of the complexes was determined using the commercial WST-1 cell metabolism and proliferation test. Primary screening of cytotoxic activity of 10 μM **3a–7a** and **3b–7b** was evaluated on nine distinct cancer cell lines with different tissue of origin (Table 3).

In single-dose 10 μM, the complexes containing bian (**3a**, **3b**) or 4-MeO-bian (**4a**, **4b**) as ligand have considerably higher cytotoxic effect then complexes bearing pyma (**5a**, **5b**), dppz (**6a**, **6b**) or bda (**7a**, **7b**) after 48 h incubation. The cytotoxicity effect of the tested complexes on the cell lines is also dependent on the origin of the cell line. The complexes **3a**, **3b**, **4a** and **4b** evince a very good inhibitory effect on epithelial cells HeLa and A549 or cells Saos2. However, studying these complexes, we observe also a significant cytotoxic effect on the human breast cancer MCF-7, ovarian cancer A2780 and pancreatic cancer PANC-1 cell lines. The complexes with ligand pyma (**5a**, **5b**) are the

Table 3
Primary single-dose screening of cytotoxic activity using WST-1 assay. Cells were treated by **3a–7a** and **3b–7b** complexes for 48 h at a final concentration of 10 μM. Results are the mean values ± SD of three independent replications.

	Cell lines% of inhibition								
	A2780	A549	HeLa	HT-29	Jurkat	MCF-7	MOLT-4	PANC1	Saos2
3a	91.0 ± 2.3	99.6 ± 0.1	96.6 ± 0.3	83.3 ± 1.9	81.1 ± 0.9	91.9 ± 2.0	89.5 ± 1.7	72.3 ± 6.0	97.1 ± 0.3
3b	96.3 ± 0.4	100 ± 1.4	98.5 ± 1.1	93.7 ± 2.7	98.1 ± 0.5	90.7 ± 2.7	94.2 ± 1.0	78.8 ± 4.2	95.0 ± 1.9
4a	88.8 ± 0.2	98.6 ± 0.3	96.7 ± 0.6	95.8 ± 0.6	86.4 ± 2.2	80.8 ± 9.2	92.4 ± 1.1	72.6 ± 5.4	97.3 ± 0.6
4b	91.8 ± 2.1	100 ± 0.4	100 ± 2.2	97.5 ± 0.5	97.7 ± 0.4	93.8 ± 1.7	95.4 ± 0.7	76.8 ± 5.9	99.7 ± 0.4
5a	0.0 ± 0.1	1.2 ± 0.7	0.0 ± 0.2	0.0 ± 0.1	0.0 ± 0.3	0.0 ± 0.2	16.5 ± 3.6	0.0 ± 0.1	1.2 ± 0.9
5b	0.0 ± 0.1	0.0 ± 0.5	0.0 ± 0.2	0.0 ± 0.6	0.0 ± 0.1	0.0 ± 0.2	0.0 ± 0.4	0.0 ± 0.5	0.0 ± 0.3
6a	13.5 ± 5.7	83.3 ± 7.7	66.1 ± 5.8	43.6 ± 6.1	32.3 ± 3.8	79.4 ± 1.3	80.2 ± 8.4	29.2 ± 4.1	82.8 ± 3.4
6b	35.2 ± 7.6	62.7 ± 7.9	31.3 ± 7.7	0.3 ± 5.2	0.0 ± 0.1	53.8 ± 5.0	0.0 ± 0.3	2.1 ± 12.3	36.9 ± 9.5
7a	0.0 ± 0.2	49.4 ± 2.3	55.1 ± 7.7	15.4 ± 5.3	0.0 ± 0.2	0.0 ± 0.8	8.0 ± 3.6	0.0 ± 0.2	0.0 ± 0.4
7b	0.0 ± 0.4	49.0 ± 5.2	50.4 ± 7.7	17.0 ± 5.3	0.0 ± 0.7	0.0 ± 0.3	0.0 ± 0.4	0.0 ± 0.7	7.8 ± 2.7

least sensitive ones to the cell lines. To investigate the biological activity, the complexes **3b** and **4b**, which inhibited growth of all tested cancer cell lines, were selected. Collectively, most efficient inhibition was observed in A549 cells of NSCLC. Thus, for this cell line, the dose dependency was evaluated and IC_{50} was calculated from the measured results. In the A549 cells, the determined IC_{50} was 3.3 ± 0.6 μM at 24 h and 2.9 ± 0.2 μM at 48 h for the **3b** complex, 2.1 ± 0.2 μM at 24 h and 1.6 ± 0.1 μM at 48 h for the **4b** complex and 43.5 ± 1.5 μM at 24 h and 24.0 ± 1.9 μM at 48 h for the reference drug *cis*-platin (Fig. S2 in the Supporting information). Obtained IC_{50} values were used to determine the optimal concentration range for the follow-up experiments.

3.3. Proliferation assay

Cells counts with Trypan blue dye exclusion test were performed to validate WST-1 results and to determine whether the complexes compromises cancer cells proliferation, viability or both events. Proliferation of the A549 cells treated by complexes **3b** and **4b** decreases during 24 h compared with non-treated control cells (Fig. 5). Inhibition of proliferation occurs already at concentration 1 μM **3b** to 74.4%. The cytotoxic effect clearly increases with increasing concentration of the **3b**. For 10 μM of the **3b**, the inhibition of proliferation was 19.6%. A549 cells viability was affected with significantly increased percentage of death cells after being exposed to **3b** at 5 and 10 μM in a dose-dependent manner. The inhibitory effect of the **4b** against the cells A549 is similar to the complex **3b**. With increasing amount of the **4b** complex in concentrations 1, 3, 5 and 10 μM, the proliferation activity is inhibited to 31.3%. In turn, considerable reduction of A549 cells viability is observed only after the application of complexes **3b** in 5 and 10 μM concentrations, leading to 10% and 13% of dead cells, respectively.

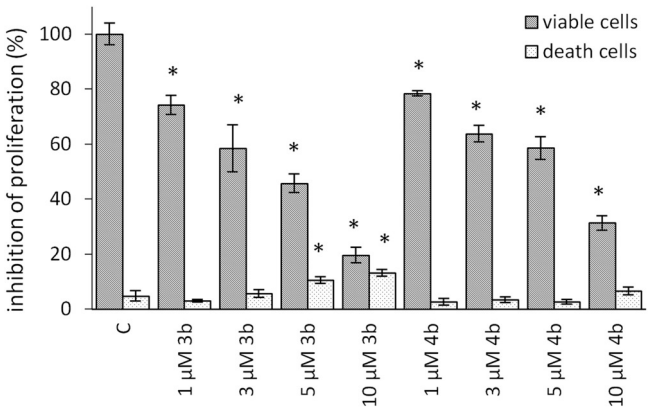

Fig. 5. The amount cells of the A549 cells after treatment with complexes **3b** and **4b** during 24 h. Results are shown as mean ± SD of three independent experiments. *Significantly different to control (C) ($P < 0.05$).

3.4. LDH activity

Results from LDH leakage assay are shown in the Fig. 6. A statistically significant LDH release from cells was observed dose-dependently at concentration 2, 4 and 6 μM of the complex **3b** providing 23% at 6 μM of **3b** at 24 h interval, whereas after 48 h, at 6 μM it was 54% which is comparable to those obtained for 40 μM of *cis*-platin. When the tested complex **4b** was applied in the concentrations 4 and 6 μM, it caused statistically significant increase of LDH release, raising the maximum LDH leakage to 18% after 24 h and to 47% after 48 h of treatment with 6 μM. The kinetic results, obtained by monitoring changes in the release of LDH between 24 and 48 h of treatment showed that LDH is released in higher amount by dying cells in a duration-dependent fashion.

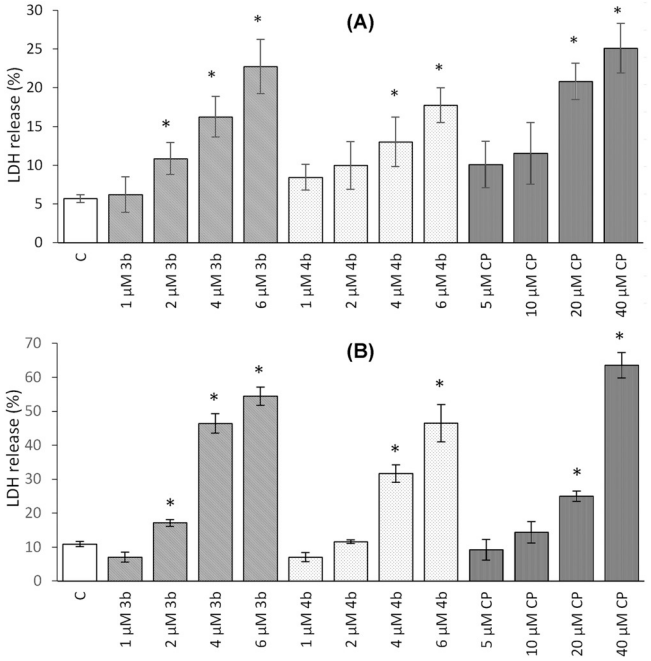

Fig. 6. The amount of LDH released from A549 cells (%) after application of test complex **3b**, **4b** and *cis*-platin (CP) for 24 h (A) and 48 h (B). Results are shown as mean ± SD of three independent experiments. *Significantly different to control (C) ($P < 0.05$).

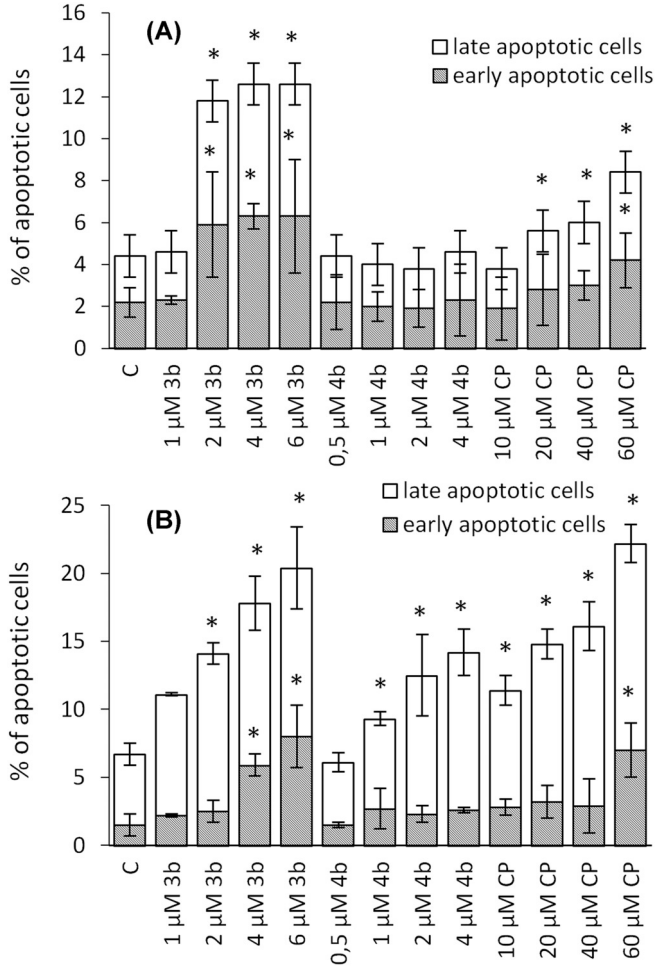

Fig. 7. Determination of apoptosis in A549 cells 24 h and 48 h after treatment with **3b**, **4b** and *cis*-platin. Determined by using the flow cytometry. Results are shown as mean of three independent experiments. *Significantly different to control (C) ($P < 0.05$).

3.5. Determination of apoptosis

The intensity of the apoptotic effect of the test complexes **3b**, **4b** and *cis*-platin in A549 cells after 24 and 48 h is shown in Fig. 7 (histograms are shown by Figs. S3 and S4 in the Supporting information). For the **3b** complex, a significant decrease of viable cells to 85.5% was detected for the concentration 2 μM during 24 h (as compared to the control 95.3%) and the amount of the late-apoptotic cells grew to the 7.1% (control 2.2%). For concentrations 4 and 6 μM, the quantity of viable cell dropped to 85.2 and 79.9% and late-apoptotic cells increased to 8.1 and 13.5%, respectively. The amount of early-apoptotic cells at group exposed to the complex **3b** is significantly higher (about 6%) compared to control (2.2%), but this amount is constant for all tested concentrations of the complex **3b**. Apoptotic effect during 48 h of exposition to the complex **3b** is comparable with 24 h of incubation. The application of the complex **4b** does not have significant effect on the A549 cells during 24 h of treatment. Although pro-apoptotic activity of the complex **4b** was confirmed at 2 and 4 μM concentrations with longer incubation times of 48 h. Additionally, the amount of late-apoptotic cells was detected 10.2 and 11.6% while reducing viable cells to 87.0% and 85.4%.

The proportions of apoptotic populations induced by *cis*-platin treatment in A549 cells were very similar to those produced by complex **3b**. However, the apoptosis occurs at higher concentrations than of the complex **3b**. After application of *cis*-platin for 24 h at 60 μM, amount of late-apoptotic cells increases to the 12.4%. Exposition for 48 h in

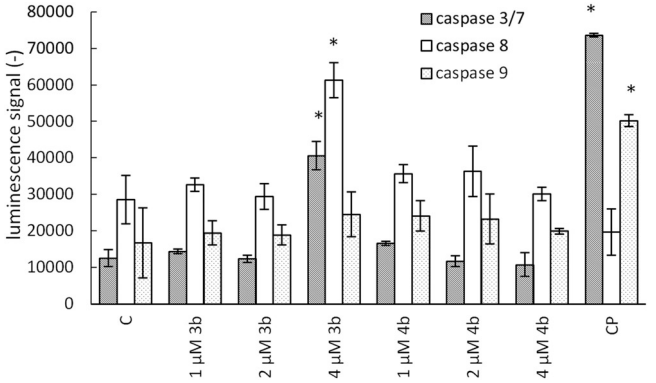

Fig. 8. Activity of caspase 3/7, caspase 8 and caspase 9 after application **3b**, **4b** and *cis*-platin (CP) on A549 cells during 24 h. Results are shown as mean ± SD of three independent experiments. *Significantly different to control (C) ($P < 0.05$).

concentration 40 μM resulted into increase of early-apoptotic cells to the 7% and late-apoptotic cells to the 15.2%. Within both investigated intervals of **3b** or *cis*-platin treatment, the amount of apoptotic cells raised with the increase of concentration or incubation time. Conversely, the pro-apoptotic effects of **4b** depends on prolonged incubation time. After incubating cells with **4b** for < 24 h, almost no apoptosis was observed. After longer times of 48 h incubation with **4b**, a dose-dependent effect on apoptosis was apparent.

3.6. Activity of caspases

A typical characteristic of apoptosis is the activation of caspases, a class of cysteine proteases that selectively cleave proteins to orchestrate programmed cell death. Fig. 8 shows activity of caspases 3/7, 8 and 9 in the A549 cells after 24 h of exposure. Concentration 4 μM of **3b** caused a significant induction of the apoptotic process. This dose caused an increase of activity of the effectors caspases 3/7 and the initiator caspase 8. At the same concentration, incubation with the complex **4b** did not cause activation of caspases within 24 h. *cis*-Platin in concentration of 40 μM was used as positive control, where its apoptotic effect is confirmed via activation of intrinsic pathway in cancer cells.

3.7. Analysis of cell cycle

Analysis of cell cycle distribution of A549 cells after 24 h and 48 h (Fig. 9) (histograms are on Figs. S5 and S6 in the Supporting information) treatment with **3b**, **4b** and *cis*-platin showed redistribution of cells in different phases of the cell cycle. The statistically significant effect of the complex **3b** appears already in the concentration 1 μM during 24 h of treatment. This concentration leads to a significant decrease to 23.9% of the S phase, while control was 31.2%. The decrease in proportion of S phase cells is constant despite increasing concentrations of **3b** to 4 and 6 μM. The **3b** at 6 μM concentration also caused G2 phase arrest to 36.1% (control 14.4%). The largest changes were registered during later interval of 48 h treatment. After application of **3b** at 2 μM after 48 h, the share of cells in G2 phase increased to 21.8% (control 14.6%). With increasing concentration to 4 and 6 μM, G2 block is more evident - 23.0 and 24.2% cells accumulated in G2, respectively. The cells in the S phase increases to 24.6 and 27.5% parallel to G2 phase. Similarly, the G2 and S accumulation was detected applying 2 and 4 μM of **4b** for 48 h. Increased percentage of S phase cells at 24 and 48 h is comparable to the complex **3b**. Known anticancer agent *cis*-platin promoted S or G2 populations, which is consistent with its effect on proliferation resulting from DNA cross-links. *cis*-Platin applied at 10 and 20 μM for 24 h significantly ($P < 0.05$) arrested cell cycle at G2 and decreased the number of cells at G1. In contrast, exposure to 40 and

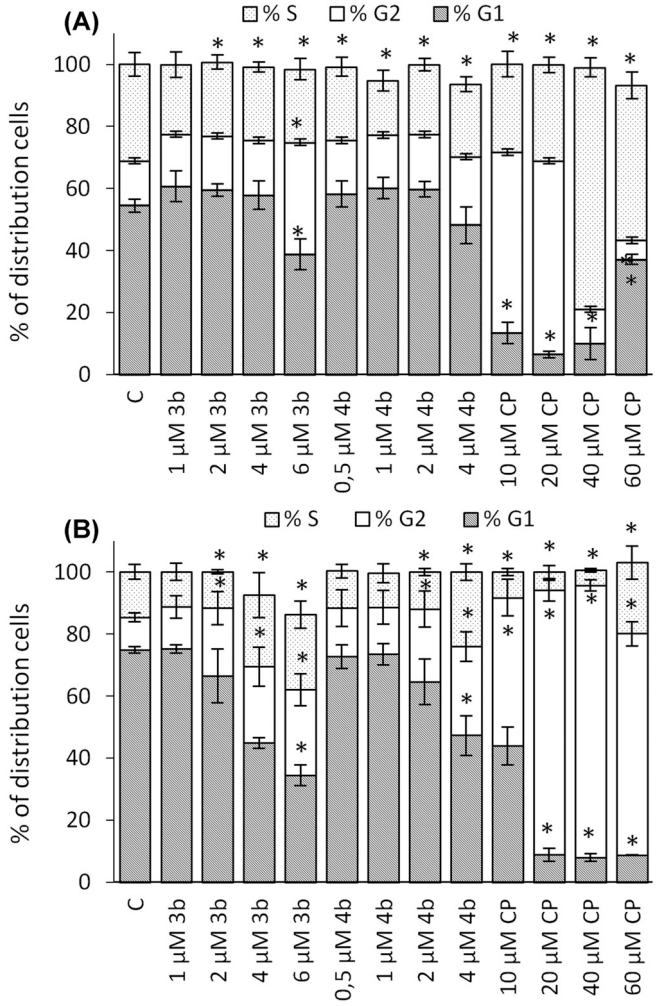

Fig. 9. The cell cycle analysis of the tested complexes **3b**, **4b** and *cis*-platin (CP) in A549 cells after 24 h (A) and 48 h (B) incubation. Results are shown as mean of three independent experiments. *Significantly different to control (C) ($P < 0.05$).

60 μM *cis*-platin for 24 h arrested the cell cycle predominately in the S phase with an increase ($P < 0.05$) from 31.2% (control) to 78.0% (40 μM) and 50.0% (60 μM). At 48 h, *cis*-platin at 5 to 20 μM induced a dose-dependent increase of G2 cells with a concomitant reduction in the proportion of cells in the G1 and S phases. Only highest concentration of *cis*-platin (40 μM) considerably increased the number of S phase cells from 14.6% (control) to 22.9%.

3.8. Electrophoresis and analysis by Western blots

The results of an analysis by Western blots used to analyze the expression level of selected proteins involved in DNA damage response, cell cycle regulation, cell death or survival in A549 cells are shown in Fig. 10. The involvement of tumor protein p53 (p53) in a signaling mechanism activated after application of complexes **3b** and **4b** was determined via p53 protein level up-regulation at 24-h interval of exposure. The level of cyclin-dependent kinase inhibitor-interacting protein 1 ($p21^{WAF1/Cip1}$) was increased at 4 h time point in **3b**, **4b** and *cis*-platin treated cells followed by further an increase at 24 h. The mitogen-activated protein kinases (MAPK) activity was studied through native extracellular signal-regulated kinases 1 and 2 (ERK1/2) as well as phosphorylated p-ERK1/2 (threonine(Thr)202/tyrosine(Tyr)204) and p38 as well as phosphorylated p-p38 (Thr180/Tyr182). Results showed an increase in the level of total protein p38 at 24 h. At the same time, the amount of p38 protein phosphorylated on Thr180/Tyr182 (p-p38) increases for all concentrations of tested complexes **3b** and **4b**. Of the regulators against apoptosis evaluated by immunoblotting, anti-apoptotic protein B-cell lymphoma (Bcl-2), showed a considerable increase when treated with **3b** and **4b**. Similarly, although no change in native ERK1/2 was detected after treatment compared with negative control, the expression levels of phosphorylated ERK1/2 (p-ERK1/2), which promote cell survival showed an increase.

Studying mechanisms by which **3b**, **4b** and *cis*-platin induce cell cycle arrest, we examined the expression levels of cell-cycle regulatory proteins. Application of **3b** and **4b** resulted in Check point kinase 1 (Chk1) phosphorylation at ser 345 (Chk1_345) from treatment time of 4 h onwards and the levels of Chk1_345 were even greater at later 24 h interval of exposure (2 and 4 μM **3b**, 1, 2 and 4 μM **4b**). The expression level of phosphorylated cell-cycle Chk2 at the Thr68 (Chk2_68) was increased at 4 h after **4b** and *cis*-platin treatment followed by an increase at 24 h, while increase in phosphorylation of Chk2 at Thr68 after exposure to **3b** was observed only in later time point of 24 h.

4. Discussion

It is known that the character of chelate ligands significantly affects cytotoxicity. Antitumor effect decreases along with 2,2′-bipyridines (bpy) and 1,10-phenanthrolines: 5-NH_2-phen > 4,7-Ph_2-phen ≈ phen > bpy ≈ 5-NO_2-phen > 5,5′-Me_2-bpy > 4,4′-Me_2-bpy ≈ 4,4′-$(MeO)_2$-bpy > 4,5-diazafluoren-9-one [17]. The highest cytotoxic effect was reached using complexes with *N*,*N*′-coordinated phen ligand and its 5-amino and 5-nitro derivatives. The IC_{50} values lies between 3.1 and 17.4 μM for MOLT-4 cells and between 2.8 and 28.2 μM for HL-60 [18]. Moreover, the apoptotic process involved in treatment-induced cell death was proved [16,35].

Ten new organometallic complexes of vanadocene with *N*,*N*′-chelating ligands were prepared and tested on nine cancer lines representing different types of cancer. It was found that the complexes containing bian or 4-MeO-bian exhibit the cytotoxic effect against the majority of the cell lines. The complexes with dppz were less effective in cytotoxic activity and the lowest cytotoxic effect to the determined cancer cells have the complexes with pyma. The results are in good agreement with those of previously published study [18] that has stated that the substitution in the Cp rings with methyl group does not influence the cytotoxic effect significantly.

To clarify the mechanism of action, we selected two very effective complexes bearing bian (**3b**) and 4-MeO-bian (**4b**). The human lung adenocarcinoma cells A549 were most sensitive to this class of complexes, and were selected to study the mechanisms underlying the cytotoxic effects of complexes **3b** and **4b**.

In the present study, it was found by determining the IC_{50} values using spectrophotometric WST-1 tetrazolium salt assay that both tested complexes have slightly higher cytotoxic activity during longer incubation period of 48 h in comparison with the shorter 24 hour incubation period. The treatment of A549 cells with complex modified with methoxy groups (**4b**) exhibited slightly higher cytotoxicity than that of the parent complex **3b**. Compared to *cis*-platin, the cytotoxicity of the both complexes after 24 h of incubation is the same as cytotoxicity of *cis*-platin after 48 h. Cytotoxic effect of the complexes **3b** and **4b** was also determined by evaluating proliferation and viability of A549 cells using Trypan Blue dye exclusion staining. The amount of cells in proliferation decreases dynamically from the lowest determined concentration of 1 μM. Even though WST-1 data strongly suggested that the higher recession largely appears because of treatment with complex **4b**, cell counting showed a higher antiproliferative activity following complex **3b**. However, stopping cells reproduction is not accompanied by increased amount of cell death followed by eradication of cancer cells. The rate of A549 cell death determined as Trypan Blue dye-positive cells was significantly increased only in cells that were exposed to higher concentrations of the complex **3b**.

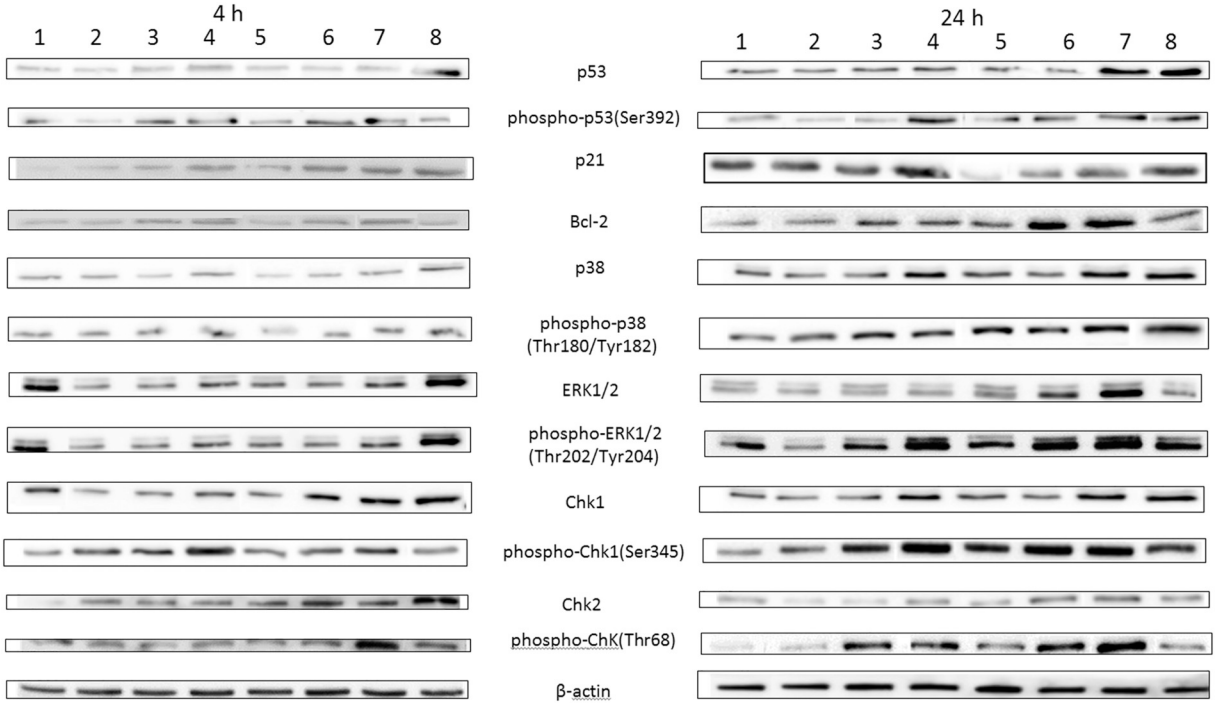

Fig. 10. Induction and activation of the proteins in the A549 cells exposed to the tested complexes at 1 μM **3b** (2), 2 μM **3b** (3), 4 μM **3b** (4), 1 μM **4b** (5), 2 μM **4b** (6), 4 μM **4b** (7), 40 μM *cis*-platin (8), (1) is untreated control. To confirm equal protein loading, membranes were reincubated with β-actin. Representative results of one of three independent experiments are shown.

Similarly, because of plasma membrane damage of A549 cells the cytoplasmic enzyme LDH is released into the cell culture medium. In conformity with viability test using Trypan Blue uptake, the higher amount of lactate dehydrogenase released after damage on cell membranes occurs after treatment with complex **3b**.

Since the vast majority of cytotoxic chemotherapeutics used in anticancer treatment acts by promoting apoptosis, a part of this work was focused on the study of the cell death mechanism following **3b** and **4b**. At present, the exact mechanism of the cytotoxic effect of vanadocene complexes is not known. However, in recent literature the multifactorial effect of the vanadocene complexes is described [36–38]. While primary studies report about interaction with α-amino acids [39,40] and suggest inhibitory effect on enzymes protein kinase C and topoisomerase II [41,42]. In another study, treatment-induced inhibition/activation of tyrosin phosphorylase leads to the tumor suppressor gene activation accompanied by DNA damage and lipoperoxidation of plasmatic membrane due to production of free radicals [43]. This effect is supported using the oncolytic virus [44]. Newer studies on vanadocene complexes with *N*,*N′*-chelate describe intercalation into DNA [45], cleavage of pBR322 plasmid DNA [46] and also show DNA photocleavage activity in infrared light via hydroxyl radical pathway [47].

It could be noted that vanadocene compounds bearing chelating ligands, including here reported derivatives, are considerably more hydrolytically stable than parent dichloride (**1a**), which splits off the chloride ligands immediately after dissolution in water or in other therapeutic media [13,48]. Although exact speciation after biological metabolic processing was not clarified, longer survive in the biological environment could be one of the basic reasons responsible for observed higher effectivity [49].

We suppose that important molecular target of the cytotoxic effect of the tested complexes **3b** and **4b** is protein p53. Similarly, p53 was up-regulated after *cis*-platin treatment and thus *cis*-platin share with **3b** and **4b** p53 as the molecular target [50]. Posttranslational modification of p53 by phosphorylation at ser392 proved the stabilization of p53 in both **3b** and **4b** treated A549 cells. Bonding of phosphate to ser392 in p53 creates a stable tetrameric form of protein, which is necessary to activate transcription of p53-dependent cell cycle regulating or apoptotic genes in response to DNA damage [51]. Among these, up-regulation of p53 is also closely connected with increase of transcriptional activity of protein $p21^{WAF1/Cip1}$ and it acts as an important mediator of p53 tumor suppressor activity [52]. Increased amount of cyclin-dependent kinase inhibitor $p21^{WAF1/Cip1}$ was also detected in A549 cells after treatment with complexes **3b** and **4b**. Radical changes in the amount of protein p53, $p21^{WAF1/Cip1}$ and subsequent increase in the level of Chk1 and Chk2 and their phosphorylated forms of Chk1 at ser345 and Chk2 at Thr68 significantly affected cell cycle progression. Since $p21^{WAF1/Cip1}$ works as inhibitor of cyclin dependent kinase, its excessive up-regulation decreases the expression of gene for the cell cycle progression [53]. Cell cycle analysis revealed that treatment of A549 cells with the complexes **3b** and **4b** caused cell cycle delay at the G2/M restriction point with increased percentage of G2 phase cells. Our results showed that **3b** and **4b** induced inhibitory effect on A549 viability and plasma membrane integrity was due to apoptosis activation. This is supported by our data showing that treatment with complex **3b** leads to the activation of the initiator caspase (caspase 8), which then cleaves and activates the effector caspases (caspases 3/7). Apoptosis was next determined using quantification of Annexin-V positive cells, showing that both complexes increased the percentage of Annexin-V-binding cells compared to negative control. To provide comprehension of the mechanisms associated with induction of apoptosis, the molecular basis of apoptosis mediated by complexes **3b** and **4b** was investigated. This pro-apoptotic effect seems to be mediated by up-regulation of MAPK activity and increase in the amount of p38 protein. We also looked for the direct involvement of mitochondria in apoptotic process by evaluating effect of treatment on the protein Bcl-2. This protein acts as an inhibitor of apoptosis as it prevents release of apoptogenic factors, such as the cytochrome *c* and apoptosis-inducing factor, and thus suppressing a downstream step, which leads to the activation of caspases [54]. Additionally, the reparation of cell damage occurs as a compensatory response to stress conditions by activating intracellular signaling mechanisms that promote cells survival. In this regard, the cells accumulate in the S phase of the cell cycle supported by

activation of ERK1/2 where its effect is connected with cell proliferation and antiapoptotic function [55].

5. Conclusion

We report remarkable cytotoxic effect of newly synthesized vanadocene complexes with *N*,*N*′-chelating ligands. Elemental analysis, mass spectrometry, infrared and EPR spectroscopy of these complexes was performed. Superior cytotoxicity was found in complexes with bian, 4-MeO-bian and pyma. The most cytotoxic active tested complexes are the compounds $[(\eta^5\text{-}C_5H_4Me)_2V(bian)][OTf]_2$ (**3b**) and its modified complex with methoxy groups $[(\eta^5\text{-}C_5H_4Me)_2V(4\text{-}MeO\text{-}bian)][OTf]_2$ (**4b**). From the primary cytotoxicity screening, it was proved that the most sensitive cells are the human lung adenocarcinoma cells A549; therefore, detailed investigations were performed with A549.

Mechanisms of action of **3b** and **4b** is dependent on the protein p53 following the mode of action of *cis*-platin. The up-regulation of $p21^{WAF1/Cip1}$, activation of checkpoint kinases and regulation the cell cycle occurs. Both complexes have a considerable dose-dependent antiproliferative effect, which delayed cell cycle progression by accumulating A549 cells in the G2 phase. Decrease of viability of A549 and LDH release is given by activation of apoptotic process via activation of caspases 8 and 3/7. Apoptosis is support of activation MAP kinases activity and protein p38. However, apoptosis is partially inhibited due to an increase in the amount of antiapoptotic factor Bcl-2. The A549 cells treated with **3b** and **4b** showed up-regulation of ERK1/2 protein levels, whereby increase percentage of S phase cells. Nevertheless, the cytotoxicity of the both complexes is higher, compared with *cis*-platin, and occurs already after 24 h incubation of A549 with the test compounds in a time dependent fashion. The test compounds, especially **3b**, is worthy of further study and can be developed into a new anticancer drug against lung adenocarcinoma.

Abbreviations

Bcl-2	B-cell lymphoma 2
bpy	2,2′-bipyridine
bda	benzene-1,2-diamine
bian	1,2-bis(phenylimino)acenaphthene
ChK	check point kinases
C	control
CP	*cis*-platin
Cp	cyclopentadienyl
dppz	dipyrido[3,2-*a*:2′,3′-*c*]phenazine
EtOH	ethanol
EPR	electron paramagnetic resonance
HFC	hyperfine coupling
FITC	fluorescein isothiocyanate
IC_{50}	half-maximal inhibitory concentration
LDH	lactate dehydrogenase
MAPK	mitogen-activated protein kinases
4-MeO-bian	1,2-bis(4-methoxyphenylimino)acenaphthene
4,4′-Me_2-bpy	4,4′-dimethyl-2,2′-bipyridine
5,5′-Me_2-bpy	5,5′-dimethyl-2,2′-bipyridine
4,4′-$(MeO)_2$-bpy	4,4′-dimethoxy-2,2′-bipyridine
MS	mass spectrometry
5-NH_2-phen	5-amino-1,10-phenanthroline
5-NO_2-phen	5-nitro-1,10-phenanthroline
NSCLC	non-small cell lung cancer
$p21^{WAF1/Cip1}$	cyclin-dependent kinase inhibitor-interacting protein 1
p53	tumor protein p53
phen	1,10-phenanthroline
4,7-Ph_2-phen	4,7-diphenyl-1,10-phenanthroline
pyma	(*E*)-*N*-((pyridin-2-yl)methylene)benzenamine
SD	standard deviation
Ser	serine
THF	tetrahydrofuran
Thr	threonine
Tyr	tyrosine
WST-1	2-(4-iodophenyl)-3-(4-nitrophenyl)-5-(2,4-disulfophenyl)-*2H*-tetrazolium sodium salt

Acknowledgement

This work was supported by the program UPA SG380006 and Progres/UK Q40/01. We wish to thank Ms. Naděžda Mazánková for her skillful technical assistance.

Appendix A. Supplementary material

Supplementary data to this article can be found online at https://doi.org/10.1016/j.jinorgbio.2019.03.015.

References

[1] R.A. Juergens, J.R. Brahmer, J. Natl. Compr. Cancer Netw. (4) (2006) 595–600.
[2] W. D. Travis, E. Brambilla, M. Noguchi, A. G. Nicholson, K. R. Geisinger, Y. Yatabe, D. G. Beer et. al., J. Thorac. Oncol. 6 (2011) 244–285.
[3] J. Brognard, A.S. Clark, Y. Ni, P.A. Dennis, Cancer Res. 61 (2001) (3986–399).
[4] D.M. Parkin, F. Bray, J. Ferlay, P. Pisani, CA Cancer J. Clin. 55 (2005) 74–108.
[5] American Cancer Society, Cancer Facts and Figures 2007, American Cancer Society, Atlanta, 2007.
[6] L. Ding, G. Getz, D. A. Wheeler, E. D. Mardis, M. D. McLellan, K. Cibulskis, C. Sougnez, H. Greulich, D. M. Muzny et al., Nature 455 (2008) 1069–1075.
[7] T. Takahashi, N.N. Nau, I. Chiba, M.J. Birrer, R.K. Rosenberg, M. Vinocour, M. Levitt, H. Pass, A.F. Gazdar, J.D. Minna, Science 246 (1989) 491–494.
[8] T. Mitsudomi, S. Morita, Y. Yatabe, S. Negoro, I. Okamoto, J. Tsurutani, T. Seto, M. Satouchi, H. Tada, T. Hirashima, K. Asami, N. Katakami, M. Takada, H. Yoshioka, K. Shibata, S. Kudoh, E. Shimizu, H. Saito, S. Toyooka, K. Nakagawa, M. Fukuoka, Lancet Oncol. 11 (2010) 121–128.
[9] W. Zhu, X.M. Wang, L. Zhang, X.Y. Li, B.X. Wang, Am. J. Chin. Med. 33 (2005) 839–850.
[10] C.A. Rabik, M.E. Dolan, Cancer Treat. Rev. 33 (2007) 9–23.
[11] P.K. Sasmal, S. Saha, R. Majumdar, R.R. Dighe, A.R. Chakravarty, Inorg. Chem. 49 (2010) 849–859.
[12] J. Honzíček, I. Klepalová, J. Vinklárek, Z. Padělková, I. Císařová, P. Šiman, M. Řezáčová, Inorg. Chim. Acta 373 (2011) 1–7.
[13] J. Honzíček, J. Vinklárek, Inorg. Chim. Acta 437 (2015) 87–94.
[14] M.S. Murthy, J.H. Toney, L.N. Rao, L.Y. Kuo, T.J. Marks, Proc. Am. Assoc. Cancer Res. 27 (1986) 279.
[15] P. Köpf-Maier, B.K. Keppler (Ed.), Metal Complexes in Cancer Chemotherapy, VCH, Weinheim, 1993, pp. 259–296.
[16] L. Šebestová, R. Havelek, M. Řezáčová, J. Honzíček, Z. Kročová, J. Vinklárek, Chem. Biol. Interact. 242 (2015) 61–70.
[17] L. Šebestová, J. Vinklárek, J. Honzíček, Z. Růžičková, M. Řezáčová, Inorg. Chim. Acta 427 (2015) 211–218.
[18] J. Vinklárek, H. Hurychová, J. Honzíček, L. Šebestová, Z. Padělková, M. Řezáčová, Eur. J. Inorg. Chem. 14 (2013) 2665–2672.
[19] D.C. Crans, J.J. Smee, E. Gaidamauskas, L. Yang, Chem. Rev. 104 (2004) 849–902.
[20] S. Cuesta, D. Francés, G.B. García, Neurotoxicol. Teratol. 33 (2011) 297–302.
[21] A.M.A. Adam, A.M. Naglah, M.A. Al-Omar, M.S. Refat, Int. J. Immunopathol. Pharmacol. 30 (2017) 272–281.
[22] T. Scior, J.A. Guevara-Garcia, Q.-T. Do, Curr. Med. Chem. 23 (2016) 2874–2891.
[23] J.C. Pessoaa, S. Etcheverry, D. Gambinoc, Chem. Rev. (2015) 301–302 (24–48).
[24] M.S. Molinuevo, A.M. Cortizo, S.B. Etcheverry, Cancer Chemother. Pharmacol. 61 (2008) 767–773.
[25] I.E. Leon, V. Porro A.L. Di Virgilio, L.G. Naso, P.A. Williams, M. Bollati-Fogolín, S.B. Etcheverry, J. Biol. Inorg. Chem. 19 (2014) 59–74.
[26] W.L.F. Armarego, D.D. Perrin (Eds.), Purification of Laboratory Chemicals, Butterworth-Heinemann, Oxford, 1996.
[27] G. Wilkinson, J.M. Birmingham, J. Am. Chem. Soc. 76 (1954) 4281–4284.
[28] J.L. Petersen, L.F. Dahl, J. Am. Chem. Soc. 97 (1975) 6422–6433.
[29] M.J. Edelmann, J.-M. Raimundo, N.F. Utesch, F. Diederich, C. Boudon, J.-P. Gisselbrecht, M. Gross, Helv. Chim. Acta 85 (2002) 2195–2213.
[30] M. Gasperini, F. Ragaini, S. Cenini, Organometallics 21 (2002) 2950–2957.
[31] G.M. Sheldrick, Acta Crystallogr. Sect. A A71 (2015) 3–8.
[32] G.M. Sheldrick, Acta Crystallogr. Sect. C C71 (2015) 3–8.
[33] P. Ghosh, A.T. Kotchevar, D.D. DuMez, S. Ghosh, J. Peiterson, F.M. Uckun, Inorg. Chem. 38 (1999) 3730–3737.
[34] F.H. Allen, Cambridge Structural Database, Acta Crystallogr. Sect. B B58 (2002) 380.
[35] O.J. D'Cruz, F.M. Uckun, J. Appl. Toxicol. 21 (2011) 331–339.
[36] A. Bishayee, A. Waghray, M. A. Patel, M. Chatterjee, Cancer Lett. 294 (2010) 1–12.
[37] J.C. Pessoa, S. Etcheverry, D. Gambino, Coord. Chem. Rev. 301 (2015) 24–48.
[38] D. Crans, L. Yang, A. Haase, X. Yang, Met. Ions Life Sci. 18 (2018) 251.
[39] J. Vinklárek, H. Paláčková, J. Honzíček, J. Holubová, M. Holčapek, I. Císařová,

Inorg. Chem. 45 (2006) 2156–2162.
[40] J. Vinklárek, H. Paláčková, J. Honzíček, Collect. Czechoslov. Chem. Commun. 69 (2004) 811–821.
[41] L.Y. Kuo, A.H. Liu, T.J. Marks, Met. Ions Biol. Syst. 33 (1996) 53–85.
[42] G. Mokdsi, M.M. Harding, J. Inorg. Biochem. 83 (2001) 205–209.
[43] A.M. Evangelou, Crit. Rev. Oncol. Hematol. 42 (2002) 249–265.
[44] M. Selman, C. Rousso, A. Bergeron, H. Son, R. Krishnan, N. El-Sayes, O. Varette, A. Chen, F. Tzelepis, J. Bell, D. Crans, J. Diallo, Mol. Ther. 26 (2018) 56–69.
[45] L. Shivakumar, K. Shivaprasad, H.D. Revanasiddappa, Spectrochim. Acta A 97 (2012) 659–666.
[46] L. Bian, L. Li, Q. Zhang, J. Dong, T. Xu, J. Li, J. Kong, Transit. Met. Chem. 37 (2012) 783–790.
[47] P.K. Sasmal, S. Saha, R. Majumdar, S. De, R.R. Dighe, A.R. Chakravarty, Dalton Trans. 39 (2010) 2147–2158.
[48] J. Honzíček, Z. Růžičková, J. Vinklárek, Inorg. Chim. Acta 453 (2016) 39–41.
[49] A. Levina, D.C. Crans, P.A. Lay, Coord. Chem. Rev. 352 (2017) 473–498.
[50] S.E. Morgan, M.B. Kastan, Adv. Cancer Res. 71 (1997) 1–25.
[51] K. Sakaguchi, H. Sakamoto, M.S. Lewis, C.W. Anderson, J.W. Erickson, E. Appella, D. Xie, Biochemistry 36 (1997) 10117–10124.
[52] A.L. Gartel, S.K. Radhakrishnan, Cancer Res. 65 (2005) 3980–3985.
[53] B.D. Chang, M.E. Swift, M. Shen, J. Fang, E.V. Broude, I.B. Roninson, Proc. Natl. Acad. Sci. U. S. A. 99 (2002) 389–394.
[54] J. Yang, X. Liu, K. Bhalla, C.N. Kim, A.M. Ibrado, J. Cai, T.I. Peng, D.P. Jones, X. Wang, Science 275 (1997) 1129–1132.
[55] S.E. Golding, E. Rosenberg, S. Neill, P. Dent, L.F. Povirk, K. Valerie, Cancer Res. 67 (2007) 1046–1053.